Wireless Infrared Communication Links Using Multi-Beam Transmitters and Imaging Receivers

Andrew P. Tang, Joseph M. Kahn, and Keang-Po Ho*
Department of Electrical Engineering and Computer Sciences
University of California, Berkeley, CA 94720

Abstract

We discuss two modifications to the design of wireless infrared links that can yield dramatic performance improvements. In non-directed, non-line-of-sight (non-LOS) links, replacement of the diffuse transmitter by one that projects multiple narrow beams can reduce the path loss, typically increasing the link SNR by about 20 dB. In both non-directed, LOS and non-directed, non-LOS links, replacement of the non-imaging receiver by one employing an imaging light concentrator and a segmented photodetector can reduce received ambient light noise and multipath distortion. This can yield SNR improvements of tens of decibels.

1. Introduction

Infrared (IR) radiation is an attractive transmission medium for short-range indoor wireless communication systems [1]-[3]. The advantages of IR over radio include: (a) the availability of a vast, unregulated bandwidth, (b) freedom from multipath fading (though not multipath distortion) [4], and (c) IR is blocked by walls, providing immunity to eavesdropping and permitting reuse of the same bandwidth throughout a building.

Currently, intensity modulation with direct detection (IM/DD) is considered to be the only practical means of modulating and detecting the optical carrier. IR links using IM/DD are subject to several impairments [2],[3]. (a) Steady ambient IR sources, such as sunlight and incandescent lighting, induce high-intensity shot noise in the receiver. (b) Fluorescent lamps emit IR that is modulated periodically at the lamp drive frequency, causing interference that lies between near-d.c. and about 1 MHz. (c) The receiver electrical signal-to-noise ratio (SNR) is proportional to the square of the received optical power, while the available transmitter power is limited by concerns of power consumption and eye safety, particularly in portable transmitters. (d) The received power can be increased by use of a large-area detector in conjunction with an optical concentrator [5],[6]. However, the resulting high detector capacitance leads to an increase in the input-referred receiver thermal noise [7],[8]. (e) The use of non-directional transmitters and receivers leads to multipath distortion, which impairs digital communication at bit rates above approximately 10 Mb/s [4].

Traditionally, IR links have been classified [2] according to whether they employ a directional or non-directional transmitter and receiver, and whether or not they rely upon the existence of an uninterrupted line-of-sight (LOS) path between the transmitter and the receiver. At present, directed, LOS links are the most widely used. Because they employ directional transmitters and receivers, the path loss is small, and multipath distortion is usually negligible. Another popular link design is the non-directed, non-LOS link (often referred to as a *diffuse link*). The diffuse transmitter is highly non-directional, as it relies upon diffuse reflection of light from an extended surface, such as a ceiling. Diffuse links typically employ non-directional receivers. While diffuse link design alleviates the need for aiming of the transmitter at the receiver, and provides some immunity to blockage of the transmission path, it results in a high path loss, requiring a high transmitter power.

In this paper, we analyze the use of imaging receivers in IR links, showing that they yield large improvements in SNR over their non-imaging counterparts. We define an *imaging receiver* to be one that employs a single imaging optical concentrator (e.g., lens) in conjunction with a detector segmented into multiple pixels. By contrast, a *non-imaging receiver* employs an optical concentrator (usually non-imaging) with a single detector. We note that many of the benefits of the imaging receiver can be realized through use of a collection of narrow-acceptance-angle, non-imaging receivers oriented in different directions [9], but the imaging receiver requires only a single concentrator and a planar detector array, facilitating the use of many pixels. Furthermore, for the case of non-directed, non-LOS links, we analyze the use of a *quasi-diffuse transmitter*, which replaces the single wide beam of the diffuse transmitter by a collection of differently oriented, narrow beams [10]. We show that this transmitter provides a large SNR improvement in conjunction with a non-imaging receiver, and an even larger SNR gain when used with an imaging receiver.

2. Non-Imaging and Imaging Receivers

In this section, we discuss the optical concentration ratios of non-imaging and imaging receivers, which are depicted in Fig. 1(a) and (b), respectively. Considering both types of receivers, we suppose that the concentrator input medium (typically air) has a refractive index of unity and the output medium has a refractive index of N. The concentrator has an input acceptance semiangle θ_a, and θ_o is the largest angle of all output rays. The light source subtends a semiangle θ_i. (For the moment, we neglect the weak and strong ambient light sources indicated in Fig. 1(a) and (b), which will be treated in Section 3 using the results of this section.) The thermodynamic-limited optical gain is defined to be the maximum achievable increase of irradiance between the concentrator input and output. For a light source subtending a semiangle θ_i, this is given by [5]

*Present address: Bell Communications Research, NVC 3X155, 331 Newman Springs Road, Red Bank, NJ, 07701.

To be presented at IEEE International Conference on Communications, Dallas, Texas, June 23-27, 1996

0-7803-3250-4/96$5.00©1996 IEEE

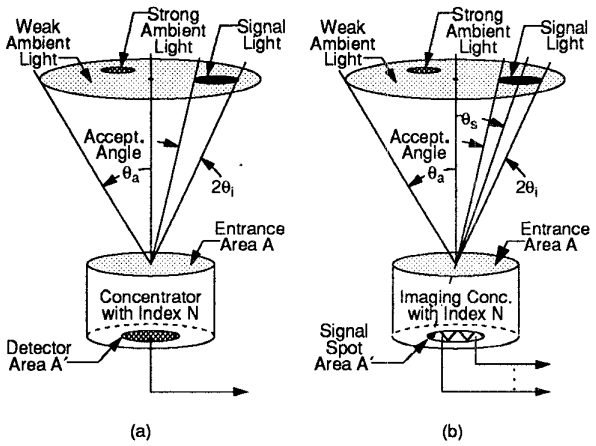

Fig. 1. Non-imaging and imaging optical receivers. (a) The non-imaging receiver employs a concentrator (usually non-imaging) in conjunction with a single detector. (b) The imaging receiver employs an imaging concentrator and a detector segmented into multiple pixels.

$$C = \frac{A}{A'} = \left(\frac{N \sin\theta_o}{\sin\theta_i}\right)^2. \quad (1)$$

Clearly, θ_o can not exceed $\pi/2$, so the theoretical maximum concentration ratio is

$$C_{max} = \left(\frac{N}{\sin\theta_i}\right)^2. \quad (2)$$

As an example, if $\theta_i = 2°$, then $C_{max} = 821N^2$.

In the case of the non-imaging receiver shown in Fig. 1(a), usually the input acceptance angle θ_a is not made very small, to alleviate the requirement for careful aiming of the receiver. The concentration ratio achieved by the non-imaging receiver cannot exceed

$$C_{max,\,NIMG} = \left(\frac{N}{\sin\theta_a}\right)^2. \quad (3)$$

For example, the non-directional hemispherical concentrator [2] achieves an acceptance semiangle $\theta_a = 90°$ and a concentration ratio $C_{hemisphere} = N^2$. The compound parabolic concentrator and lens-flowline concentrator [5] are typically designed to be more directional. As a typical example, a CPC having $\theta_a = 15°$ yields a concentration ratio $C_{15°\,CPC} = 14.9N^2$. When used with a source subtending a very small angle θ_i, these concentrators achieve concentration ratios far below the thermodynamic limit.

Considering the imaging receiver depicted in Fig. 1(b), the maximum concentration ratio is A/A', where A is the concentrator entrance area and A' is the area of the received signal spot on the detector. Assuming a distortionless imaging system and considering a possibly curved image plane, using the concept of generalized etendue [5], we obtain the maximum possible concentration ratio

$$C_{max,\,IMG} = \left(\frac{N}{\sin\theta_i}\right)^2. \quad (4)$$

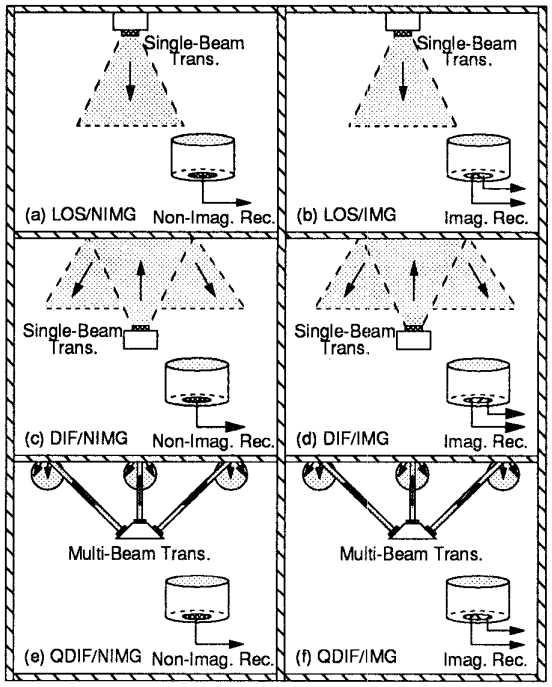

Fig. 2. Classification of links using non-imaging and imaging receivers. (a) Line-of-sight/non-imaging. (b) Line-of-sight/imaging. (c) Diffuse/non-imaging. (d) Diffuse/imaging. (e) Quasi-diffuse/non-imaging. (f) Quasi-diffuse/imaging.

(We note that our definition of concentration ratio is slightly different from that in [5]). Comparing (4) and (2), we see that the imaging receiver can achieve the thermodynamically limited concentration ratio. In principle, the imaging receiver can achieve this concentration ratio simultaneous with achieving a large acceptance angle θ_a. When the angle θ_i subtended by the source is small, the concentration ratio of the imaging receiver greatly exceeds that of the non-imaging receiver.

3. Links Using Non-Imaging and Imaging Receivers

In this section, we analyze the SNR of IR links, comparing the performance achieved with non-imaging and imaging receivers. Section 3.1 considers LOS links, while Section 3.2 treats non-LOS links, considering those employing both diffuse and quasi-diffuse transmitters.

3.1 Line-of-Sight Links

A LOS/non-imaging (LOS/NIMG) link is shown in Fig. 2(a), while a LOS/imaging (LOS/IMG) link is depicted in Fig. 2(b). In both LOS/NIMG and LOS/IMG links, path loss and multipath distortion are minimized by the use of a directional transmitter. In the case of the LOS/NIMG link, the receiver concentration ratio, and thus the link SNR, is maximized by the use of a directional receiver. For the LOS/IMG link, we will see that a high concentration ratio, and thus a high SNR, can be achieved simultaneous with a large receiver acceptance angle.

We analyze the performance of the LOS/NIMG and LOS/IMG links making reference to Fig. 1(a) and (b), respectively. For both types of links, we make the following assumptions. Signal radiation, incident at angle θ_s, and distributed uniformly over a small semiangle, θ_i, is incident with radiance B_s (W/m^2-sr) upon the optical concentrator. Following [11], we consider both localized and distributed ambient radiation sources. Strong ambient light, incident at an angle θ_{bs} and distributed uniformly over a small semiangle θ_{bsi}, is received with radiance B_{bs}. Weak ambient light, distributed uniformly over the entire acceptance angle θ_a, is received with radiance B_{bw}. As θ_a is not small, it is necessary to assume a specific angular distribution for the weak ambient radiation, and we assume it is Lambertian. A well-designed receiver will employ an optical filter to reduce the received ambient light, and the values of B_s, B_{bs} and B_{bw} are specified at the output of this filter.

We assume that both the non-imaging and imaging concentrators have equal entrance areas A. We assume that θ_i is sufficiently small that all of the received signal is imaged to a single pixel in the imaging receiver. When θ_i is small, the signal power received in both LOS/NIMG and LOS/IMG links is

$$P_{sig} = 4\pi A B_s \cos\theta_s \sin^2\left(\frac{\theta_i}{2}\right). \quad (5)$$

The total ambient power received by the detector in both types of receivers is denoted by the general symbol P_b. In the non-imaging receiver, the power received from the weak ambient source can be computed to be $\pi A B_{bw} \sin^2\theta_a$ [6], and the total detected ambient power is

$$P_{b,NIMG} = \pi A B_{bw} \sin^2\theta_a + 4\pi A B_{bs} \cos\theta_{bs} \sin^2\left(\frac{\theta_{bsi}}{2}\right). \quad (6)$$

In the imaging system, we can usually place the signal source at a different location than that of the strong ambient light source, and if the detector pixels are sufficiently small, the strong source can be rejected completely, which we assume is the case. The pixel detecting the desired signal detects only that portion of the weak ambient light that lies within the pixel. The total ambient power detected in this pixel is:

$$P_{b,IMG} = 4\pi A B_{bw} \cos\theta_s \sin^2\left(\frac{\theta_{a\text{-}px}}{2}\right), \quad (7)$$

where $\theta_{a\text{-}px}$ is the acceptance semiangle of a single pixel. This angle can lie between 0° and θ_a, and is given by

$$\theta_{a\text{-}px} = 2\sin^{-1}\left(\frac{1}{\sqrt{J}} \sin\left(\frac{\theta_a}{2}\right)\right), \quad (8)$$

where J is the number of pixels. Since $\theta_{a\text{-}px}$ is usually much smaller than θ_a, the imaging receiver typically receives much less power from the weak ambient source than a non-imaging receiver having the same acceptance angle.

We will evaluate the performance of an on-off-keyed link, neglecting the effects of multipath distortion, and assuming that the receiver noise is dominated by ambient-induced shot noise. Following the treatment of Smith and Personick [7],[8], we assume that the bit rate is B, and that rectangular pulses having duration $1/B$ are transmitted. The receiver equalizes the received pulse shape to a raised-cosine having 100% excess bandwidth. The input-referred variance of the receiver noise is given by

$$\langle i^2 \rangle_T = \langle i^2 \rangle_{shot} = 2qI_2 P_b r B, \quad (9)$$

where q is the electronic charge, r is the detector responsivity, and $I_2 = 0.562$. The average electrical SNR of the direct-detection receiver is

$$SNR = \frac{(rP_{sig})^2}{\langle i^2 \rangle_T} = \frac{rP_{sig}^2}{2qBI_2 P_b} = \alpha \frac{P_{sig}^2}{P_b}, \quad (10)$$

where $\alpha = r/2qBI_2$. The bit-error rate (BER) is given by $BER = Q(\sqrt{SNR})$, so that a SNR of 36 (15.6 dB) is required to achieve 10^{-9} BER. The SNR of the non-imaging receiver is

$$SNR_{LOS/NIMG} = \frac{16\pi\alpha A B_s^2 \cos^2\theta_s \sin^4\left(\frac{\theta_i}{2}\right)}{B_{bw}\sin^2\theta_a + 4B_{bs}\cos\theta_{bs}\sin^2\left(\frac{\theta_{bsi}}{2}\right)}, \quad (11)$$

while that of the imaging receiver is

$$SNR_{LOS/IMG} = \frac{4\pi\alpha A B_s^2 \cos\theta_s \sin^4\left(\frac{\theta_i}{2}\right)}{B_{bw}\sin^2\left(\frac{\theta_{a\text{-}px}}{2}\right)}. \quad (12)$$

Comparing (11) and (12), we see that the SNRs of the imaging and non-imaging receivers differ by a factor

$$\frac{SNR_{LOS/IMG}}{SNR_{LOS/NIMG}} = \frac{B_{bw}\sin^2\theta_a + 4B_{bs}\cos\theta_{bs}\sin^2\left(\frac{\theta_{bsi}}{2}\right)}{4B_{bw}\cos\theta_s \sin^2\left(\frac{\theta_{a\text{-}px}}{2}\right)}. \quad (13)$$

In order to simplify comparison of the SNRs, we neglect the strong ambient light source (which will underestimate the improvement obtained using LOS/IMG), neglect the factor $\cos\theta_s$ (which is of order unity), and assume that $\theta_{a\text{-}px}$ is small, in which case (13) becomes:

$$\frac{SNR_{LOS/IMG}}{SNR_{LOS/NIMG}} \approx \frac{\sin^2\theta_a}{\sin^2\theta_{a\text{-}px}}. \quad (14)$$

We see that when $\theta_{a\text{-}px} \ll \theta_a$, the imaging receiver achieves a much higher SNR than the non-imaging receiver. While (14) suggests that it is best to make $\theta_{a\text{-}px}$ as small as possible, a choice of $\theta_{a\text{-}px}$ very small may require the use of many pixels, increasing receiver complexity. In addition, assuming we use only the signal from a single detector pixel, we wish to maintain the condition that $\theta_{a\text{-}px} \geq \theta_i$, so that no signal power is lost. θ_i cannot be made infinitesimally small, because of eye-safety requirements.

In order to provide a specific example, we assume a generalized Lambertian transmitter, whose radiance is modeled as [1]

$$B_s(\phi) = \frac{n+1}{2\pi} E_{trs} \cos^{n-1}\phi, \quad (15)$$

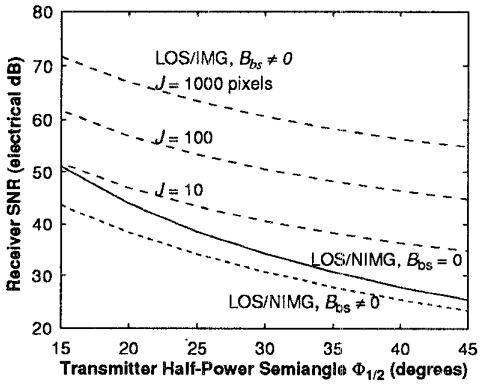

Fig. 3. Electrical SNR of line-of-sight/imaging and line-of-sight/non-imaging links, as a function of transmitter half-power semiangle $\Phi_{1/2}$. Ambient-induced shot noise is assumed to dominate the receiver noise. Ambient light includes a uniform, weak component, as well as a localized, strong component described by *Bbs*. The 100 Mb/s, on-off-keyed transmitter emits an average power of 100 mW. The link transmission distance is 3 m. The non-imaging receiver has an acceptance semiangle θ_a matched to the transmitter half-power semiangle $\Phi_{1/2}$. The imaging receiver has an acceptance semiangle $\theta_a = 45°$.

where E_{trs} is the irradiance of the transmitter, ϕ is the angle with respect to the transmitter surface normal, and the order n is related to the half-power semiangle $\Phi_{1/2}$ by

$$n = -\frac{0.693}{\ln[\cos(\Phi_{1/2})]}. \tag{16}$$

We assume that the transmitter and receiver are aligned along the same axis, so that $\theta_s = 0°$ and $\phi = 0°$. The transmitter radius is 5 cm. In order to illustrate the transition from a directional LOS system to a non-directional LOS system, we vary $\Phi_{1/2}$, and we match the acceptance angle of the non-imaging receiver to the source, i.e., $\theta_{a,NIMG} = \Phi_{1/2}$. In all cases, we assume that the imaging receiver has an acceptance angle $\theta_{a,IMG} = 45°$. Both non-imaging and imaging receivers have an entrance area $A = 9\pi/4$ cm^2 and employ an optical bandpass filter having a half-power bandwidth of 50 nm. Assuming mixed daylight and artificial illumination [1], the radiance of the weak ambient light is $B_{bw} = 1 \times 10^{-4}$ W/(cm^2 · sr). The strong ambient light, assumed to be skylight, subtends a semiangle $\theta_{bsi} = 10°$ and is received with a radiance $B_{bs} = 1 \times 10^{-3}$ W/(cm^2 · sr). The bit rate is B = 100 Mb/s, and the detector responsivity is r = 0.5A/W.

Fig. 3 displays the SNR of LOS links using non-imaging and imaging receivers as a function of the transmitter semiangle $\Phi_{1/2}$. This figure assumes an average transmitted power of 100 mW and a transmitter-receiver separation of 3 m. In all cases, as $\Phi_{1/2}$ is reduced, the received signal power increases, leading to an increase in the SNR. Considering the non-imaging receiver, when the strong ambient source is neglected ($B_{bs} = 0$), as $\theta_{a,NIMG} = \Phi_{1/2}$ decreases, the received ambient power decreases, further enhancing the SNR. When the strong ambient source is included ($B_{bs} \neq 0$), as $\theta_{a,NIMG} = \Phi_{1/2}$ decreases, the total received ambient power does not decrease as much, so the SNR increases more slowly. In the case of the imaging receiver,

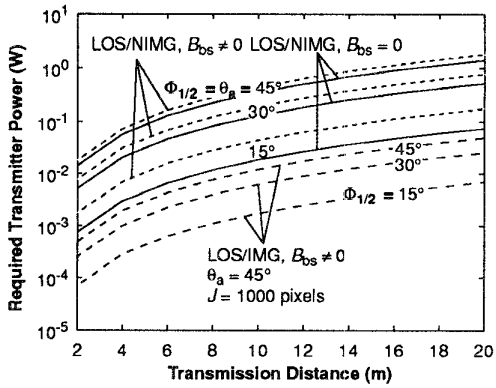

Fig. 4. Average transmitter power required for line-of-sight links to achieve 10^{-9} bit-error rate using on-off keying at 100 Mb/s, as a function of the distance between the transmitter and the receiver. In the case of non-imaging receivers, the input semiangle θ_a is matched to the transmitter half-power half-angle $\Phi_{1/2}$. All imaging receivers employ $\theta_a = 45°$ and J = 1000 pixels. All other parameters are identical to those in Fig. 3.

because $\theta_{a,IMG}$ is held constant at 45°, the received ambient power does not change as $\Phi_{1/2}$ is reduced, so that the SNR increases at a rate similar to the case of the non-imaging receiver with $B_{bs} \neq 0$. As compared to the non-imaging receiver, the imaging receiver with J = 10 pixels provides an 8-to-11-dB SNR improvement. Each tenfold increase in the pixel count provides an additional 10-dB SNR increase. In Fig. 4, we present the average transmitter power required to achieve 10^{-9} BER, as a function of link transmission distance, for non-imaging and imaging receivers. The imaging receiver is assumed to employ J = 1000 pixels. For a given value of $\Phi_{1/2}$, use of the imaging receiver reduces the required transmitter optical power by 14 to 15 optical dB.

3.2 Non-Line-of-Sight Links

Four different types of non-LOS links are depicted in Fig. 2(c)-(f). All four designs rely upon reflection of the signal from an extended surface to provide some immunity against blockage of the path between the transmitter and receiver. Illumination of a reflecting surface by a single, wide beam creates a *diffuse* transmitter, which can be combined with either a non-imaging or imaging receiver, to create the DIF/NIMG and DIF/IMG link designs, respectively. DIF/NIMG are known to be very robust against blockage of the transmission path, but suffer from high path loss and considerable multipath distortion [2],[4]. While the DIF/IMG link might achieve a higher SNR and reduced multipath distortion, the IMG receiver is better matched to the quasi-diffuse transmitter, and we will not consider DIF/IMG links here.

Illumination of the extended reflecting surface at a collection of small spots yields the *quasi-diffuse* transmitter. Combining it with non-imaging and imaging receivers forms the QDIF/NIMG and QDIF/IMG link designs, respectively. The quasi-diffuse transmitter affords some immunity to blockage, provided that more than one illuminated spot lies within the receiver acceptance angle. As compared to the diffuse link, the quasi-diffuse

link has a much smaller path loss, because the narrow beams traverse the path between the transmitter and the illuminated spot with negligible path loss [10]. The QDIF/IMG design is expected to greatly reduce the impact of multipath distortion, since the receiver can resolve beams that have been subject to different delays. The optimum QDIF/IMG receiver would equalize the delays of the various pixel signals and combine them with weights proportional to their respective SNRs, analogous to a RAKE receiver [12]. In our analysis, we neglect multipath effects; in fact, we design the QDIF links so that only one illuminated spot generally lies within the receiver acceptance angle.

Considering the DIF/NIMG link, the received signal power P_{sig} is obtained as a double integral over each point (x, y) of the ceiling, which we assume to be a Lambertian reflector [13]:

$$P_{\text{sig, DIF/NIMG}} = Ah_2^2 \iint_{\text{ceiling}} \frac{B_s(x, y)\text{rect}(x, y)dxdy}{[h_2^2 + (x - x_2)^2 + (y - y_2)^2]^2}, \quad (17)$$

where (x_2, y_2) is the position of the receiver with respect to the transmitter; rect$(x, y) = 1$ if within receiver FOV, and 0 otherwise.

Assuming that the transmitter employs an upward-directed, first-order Lambertian source, the signal radiance is given by:

$$B_s(x, y) = \frac{\rho P_{\text{trs}} h_1^2}{\pi^2 (h_1^2 + x^2 + y^2)^2}, \quad (18)$$

where P_{trs} is the average transmitted power and the ceiling has diffuse reflectivity ρ. In order to obtain a closed-form expression for the power received in the DIF/NIMG link, we make the approximations that $r = \sqrt{(x - x_2)^2 + (y - y_2)^2} \approx h_2$ and $d_r = \sqrt{x_2^2 + y_2^2} \gg r$. The received power becomes:

$$P_{\text{sig, DIF/NIMG}} \approx \frac{A\rho P_{\text{trs}} h_1^2 \tan^2\theta_a}{\pi (h_1^2 + x_2^2 + y_2^2)^2} = \frac{A\rho P_{\text{trs}} h_1^2 \tan^2\theta_a}{\pi (h_1^2 + d_r^2)^2}, \quad (19)$$

which we note is proportional to d_r^{-4} when d_r is large. Numerical evaluation of the exact and approximate formulas, (17) and (19) gives a difference less than 2 dB. In order to get analytical expression, we will use (19) in all the calculations below.

In order to compute the signal power received in QDIF/NIMG and QDIF/IMG links, we assume that the transmitter projects a lattice of M small signal spots on the ceiling, which we assume to be a Lambertian reflector. Each spot is assumed to occupy an area small enough that it is imaged to a single pixel of the imaging receiver. In both types of links, the received signal power is:

$$P_{\text{sig, QDIF}} = \frac{A\rho P_{\text{trs}} h_2^2}{M\pi [h_2^2 + d_{\text{sr}}^2]^2}, \quad (20)$$

where d_{sr} is the horizontal distance between the nearest signal spot and the receiver. The number of spots, M, is taken to have the smallest value that will guarantee that as the receiver is moved throughout a circle of radius d_r about the transmitter, at least one spot will lie within the receiver field of view. Although M is not a continuous function of d_r, we can approximate it by $M \approx d_r^2/(\tan\theta_a h)^2$. In calculating the received power, we assume that only one signal spot falls within the receiver field of view. The signal power received in the QIDF/NIMG and QDIF/IMG links is then:

$$P_{\text{sig, QDIF}} = \frac{A\rho P_{\text{trs}} \tan^2\theta_a}{\pi d_r^2}. \quad (21)$$

We note that at large d_r, $P_{\text{sig, QDIF}}$ is proportional to d_r^{-2}, by contrast with $P_{\text{sig, DIF/NIMG}}$, which is proportional to d_r^{-4}. This difference greatly enhances the SNR of quasi-diffuse links over their diffuse counterparts.

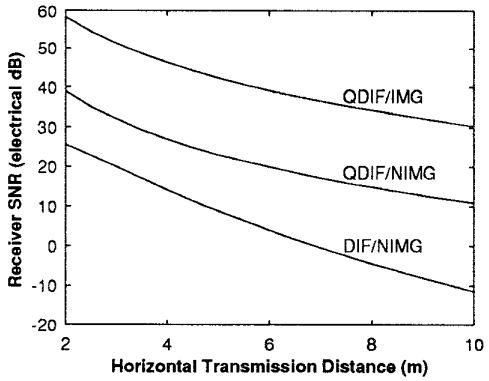

Fig. 5. Electrical SNR of diffuse/non-imaging, quasi-diffuse/non-imaging, and quasi-diffuse/imaging links, as a function of horizontal transmission distance. Ambient-induced shot noise is assumed to dominate the receiver noise. In all cases, the 100 Mb/s, on-off-keyed transmitter emits a total average power $P_{\text{trs}} = 100$ mW, the receiver has an acceptance semiangle $\theta_a = 45°$, and the transmitter and receiver are located at distances $h_1 = h_2 = 3$ m below the ceiling, which has a diffuse reflectivity $\rho = 1$. In the case of the quasi-diffuse transmitter, as the horizontal distance is increased, the number of spots, M, is increased, so as to keep one spot within the receiver field of view. In this example, M ranges from 1 to 11.

We wish to compare the SNRs achieved by the DIF/NIMG, QDIF/NIMG and QDIF/IMG links. For simplicity, we assume $\rho = 1$, $h_1 = h_2 = h$. Furthermore, we assume that $x = y = x_2 = y_2$, i.e. $d_{\text{sr}} = 0$, which corresponds to assuming that in the QDIF schemes, one signal spot lies directly above the receiver. We assume the same ambient lighting configuration as in Section 3.1, resulting in the same detected ambient power in the NIMG and IMG receivers. We thus obtain the SNR for the three types of non-LOS links:

$$SNR_{\text{DIF/NIMG}} = \frac{\alpha A P_{\text{trs}}^2 h^4 \tan^4\theta_a}{\pi^3 (h^2 + d_r^2)^4 B_{\text{bw}} \sin^2\theta_a}, \quad (22)$$

$$SNR_{\text{QDIF/NIMG}} = \frac{\alpha A P_{\text{trs}}^2 \tan^4\theta_a}{\pi^3 d_r^4 B_{\text{bw}} \sin^2\theta_a}, \quad (23)$$

$$SNR_{\text{QDIF/IMG}} = \frac{\alpha A P_{\text{trs}}^2 \tan^4\theta_a}{4\pi^3 d_r^4 B_{\text{bw}} \sin^2\left(\frac{\theta_{\text{a-px}}}{2}\right)}. \quad (24)$$

Using the same parameters assumed in Section 3.1, and assuming a ceiling height $h = 3$ m, in Fig. 5 we plot the SNR of

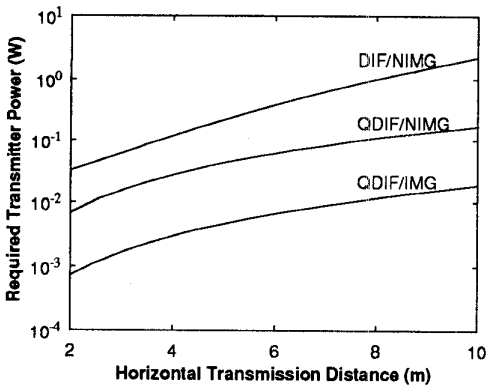

Fig. 6. Average transmitter power required for diffuse/non-imaging, quasi-diffuse/non-imaging, and quasi-diffuse/imaging links to achieve 10^{-9} bit-error rate using on-off keying at 100 Mb/s, as a function of the horizontal distance between the transmitter and the receiver. All parameters are identical to those in Fig. 5, excepting the transmitter power P_{trs}.

the three types of non-LOS links, as a function of the horizontal separation between the transmitter and receiver. Comparing the DIF/NIMG and QDIF/NIMG links, we see that the use of the quasi-diffuse transmitter greatly enhances the SNR. At large horizontal distances, where it provides the greatest reduction of path loss compared to the diffuse transmitter, it provides more than a 20-dB SNR improvement. Comparing the QDIF/NIMG and QDIF/IMG links, we note that the use of the imaging receiver provides about a 19-dB improvement of SNR over the non-imaging receiver, because of its superior rejection of ambient light. Overall, the QDIF/IMG design can provide an SNR enhancement of more than 40 dB over the DIF/NIMG design. Fig. 6 presents the average transmitter power required to achieve 10^{-9} BER, as a function of horizontal transmission distance, for the three links described in Fig. 5. The use of the QDIF/NIMG link design reduces the required power by about 10 dB over the DIF/NIMG design, while adoption of the QDIF/IMG design reduces the power requirement by approximately 10 dB more. While we have neglected multipath distortion in the above analysis, it is expected that its inclusion would further increase the advantage of the QDIF/IMG link design over the DIF/NIMG configuration.

4. Effect of Preamplifier Noise

We have neglected preamplifier noise thus far in our analysis, assuming that ambient-induced shot noise is dominant. While this assumption is often valid when non-imaging receivers are employed, the decreased ambient noise in imaging receivers can render it invalid. We will see that when preamplifier noise is included, while the optical power requirements of both non-imaging and imaging receivers increase, the advantage of imaging receivers becomes even greater, because of the reduced capacitance associated with a single detector pixel, as compared to a large-area detector.

We assume the use of a *p-i-n*/FET transimpedance receiver, and follow the analysis of Smith and Personick (see Section 3.1 and [7],[8]). We neglect the noise contributions from gate leakage current and $1/f$ noise. Including shot and thermal noises, the input-referred noise variance is given by:

$$\langle i^2\rangle_T = 2qI_2P_b rB + \frac{4kT}{R_f}I_2B + \frac{4kT\Gamma}{g_m}(2\pi C_T)^2 I_3B^3, \quad (25)$$

where the three terms represent ambient-induced shot noise, feedback-resistor noise, and FET channel noise, respectively. Here, R_f is the feedback resistance, g_m is the FET transconductance, Γ is the FET channel-noise factor, $I_2 = 0.562$, and $I_3 = 0.0868$. Neglecting stray capacitance, the total capacitance C_T is given by

$$C_T = C_d + C_g, \quad (26)$$

where C_d and C_g are the photodiode and FET gate capacitances, respectively.

We require that the transimpedance receiver have a closed-loop bandwidth equal to the bit rate B, which requires that the feedback resistance satisfy $R_f = G/2\pi BC_T$, where G is the open-loop voltage gain, which typically lies between 10 and 30. The FET noise is generally minimized when one chooses the FET to have the highest possible value of the unity-gain cutoff frequency $f_T = g_m/2\pi C_g$, and then chooses the gate capacitance to approximately equal the detector capacitance, $C_g \approx C_d$. Because of the high detector capacitances considered here, this will typically result in an FET that consumes excessive power. Therefore, to constrain the power consumption, we constrain g_m. With this constraint, for sufficiently high values of f_T, we will have $C_g \ll C_d$, allowing us to assume $C_T \approx C_d$. The total input-referred noise variance becomes:

$$\langle i^2\rangle_T \approx 2qI_2P_b rB + \frac{4kT}{G}(2\pi C_d)I_2B^2 + \frac{4kT\Gamma}{g_m}(2\pi C_d)^2 I_3B^3. \quad (27)$$

The detector capacitance Cd is proportional to the detector area A', i.e., $C_d = \varepsilon_0\varepsilon_r A'/w = \eta A'$. As in Section 2, A' is equal to the area of the total detector or one pixel in the non-imaging and imaging receivers, respectively, and can therefore be related to the concentrator input area A, acceptance semiangle θ_a, and refractive index N. For the non-imaging receiver, we obtain the total input-referred noise variance:

$$\begin{aligned}\langle i^2\rangle_{T,NIMG} = {} & 2qr\left[\pi AB_{bw}\sin^2\theta_a + 4\pi AB_{bs}\cos\theta_{bs}\sin^2\left(\frac{\theta_{bsi}}{2}\right)\right]I_2B \\ & + \frac{4kT}{G}\left(\frac{2\pi\eta A}{N^2}\sin^2\theta_a\right)I_2B^2 \\ & + \frac{4kT\Gamma}{g_m}\left(\frac{2\pi\eta A}{N^2}\sin^2\theta_a\right)^2 I_3B^3,\end{aligned} \quad (28)$$

while for the imaging receiver, the corresponding quantity is:

$$\begin{aligned}\langle i^2\rangle_{T,IMG} = {} & 2qr\left[4\pi AB_{bw}\cos\theta_s\sin^2\left(\frac{\theta_{a\text{-}px}}{2}\right)\right]I_2B \\ & + \frac{4kT}{G}\left(\frac{2\pi\eta A}{N^2}\sin^2\theta_{a\text{-}px}\right)I_2B^2 \\ & + \frac{4kT\Gamma}{g_m}\left(\frac{2\pi\eta A}{N^2}\sin^2\theta_{a\text{-}px}\right)^2 I_3B^3.\end{aligned} \quad (29)$$

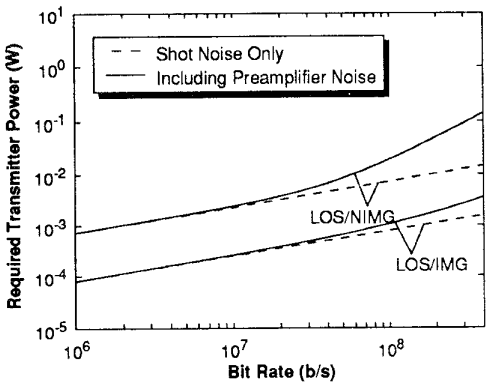

Fig. 7. Average transmitter power required to achieve 10^{-9} bit-error rate in line-of-sight/non-imaging and line-of-sight/imaging links, as a function of the bit rate. On-off keying is employed. In all cases, the transmitter half-power semiangle is $\Phi_{1/2} = 45°$, and the receiver acceptance semiangle is $\theta_a = 45°$. The concentrator refractive index is $N = 1.7$, the pixel count is $J = 100$, and the *p-i-n* detector thickness is $w = 100\ \mu m$. The transimpedance preamplifier employs a front-end FET with transconductance $g_m = 30$ mS, and achieves an open-loop voltage gain $G = 10$.

As long as $\theta_{a\text{-}px} \ll \theta_a$, the second and third terms of (29) are much smaller than those of (28), i.e., the imaging receiver has a much smaller input-referred thermal noise than the non-imaging receiver.

In order to compare the thermal noise of the two types of receivers, we consider LOS/NIMG and LOS/IMG links, with the same parameters considered in Section 3.1. We assume a transmitter half-power semiangle $\Phi_{1/2} = 45°$, a receiver acceptance semiangle $\theta_a = 45°$, a concentrator refractive index $N = 1.7$, and a pixel count $J = 100$. The detector thickness is $w = 100\ \mu m$, so that $\eta = 112$ pF/cm^2. We neglect detector transit-time effects [14], which would limit the 3-dB bandwidth of a *p*-illuminated detector of this thickness to about 440 MHz at high reverse bias. We assume a transconductance $g_m = 30$ mS, an FET channel-noise factor $\Gamma = 1.5$, and an open-loop voltage gain $G = 10$. In the imaging receiver, the area of each detector pixel is $A'_{IMG} = 0.012$ cm^2 and the associated capacitance is $C_{d,IMG} = 1.37$ pF, so that our assumption $C_{d,IMG} \gg C_g$ requires the FET cutoff frequency to satisfy $f_T \gg 3.5$ GHz. In Fig. 7, we plot the average transmitter power required for the LOS/NIMG and LOS/IMG links to achieve 10^{-9} BER, as a function of the bit rate. At a bit rate of 100 Mb/s, thermal noise induces an optical power penalty of about 1.4 dB to the LOS/IMG link, but the LOS/NIMG link incurs a penalty of about 4.1 dB. As a result, the LOS/IMG link requires about 12.7 dB less optical power than the LOS/NIMG link, a difference even greater than the 10-dB power advantage obtained neglecting thermal noise.

5. Conclusions

We have discussed two modifications to the design of wireless infrared links that can dramatically improve SNR and reduce multipath distortion. In non-directed, non-LOS links, replacement of the diffuse transmitter by the quasi-diffuse transmitter can reduce the path loss, typically increasing the link SNR by about 20 dB. In both non-directed, LOS and non-directed, non-LOS links, replacement of the non-imaging receiver by an imaging receiver can reduce received ambient light noise, yielding ambient-induced shot-noise-limited SNR improvements of tens of dB. The imaging receiver also has much lower thermal noise than the non-imaging receiver, because of the reduced capacitance associated with a single detector pixel. Finally, the imaging receiver holds promise for substantial reduction of multipath distortion. In the future, the analysis presented here should be extended to include the following considerations: (a) the potential ocular hazards associated with the quasi-diffuse transmitter, (b) computation of the exact dependence of the required number of beams, M, upon the transmission distance d_r, (c) aberrations in imaging concentrators, (d) dead zones between detector pixels, (e) detector transit time, (f) low-cost implementation of imaging receivers, and (g) multipath distortion.

6. References

1. F.R. Gfeller and U.H. Bapst, "Wireless In-House Data Communication via Diffuse Infrared Radiation," *Proc. IEEE*, vol. 67, no. 11, pp. 1474-1486, November, 1979.
2. J.R. Barry, *Wireless Infrared Communications*, Kluwer Academic Publishers, Boston, 1994.
3. J.M. Kahn, J.R. Barry, M.D. Audeh, J.B. Carruthers, W.J. Krause, G.W. Marsh, "Non-Directed Infrared Links for High Capacity Wireless LANs", *IEEE Personal Communications Magazine*, vol. 1, no. 2, pp. 12-25, May, 1994.
4. J.M. Kahn, W.J. Krause and J.B. Carruthers, "Experimental Characterization of Non-Directed Indoor Infrared Channels", *IEEE Trans. on Commun*, vol. 43, pp. 1613-1623, April, 1995.
5. W.T. Welford and R. Winston, *High Collection Nonimaging Optics*, Academic Press, San Diego, 1989.
6. R.W.Boyd, *Radiometry and the Detection of Optical Radiation*, John Wiley & Sons, New York, 1983.
7. S.D. Personick, "Receiver Design for Digital Fiber Optic Communications Systems, I and II," *Bell System Technical J.* vol 52, no. 6, pp 843-886, July-August, 1973.
8. R. G. Smith and S.D. Personick, "Receiver design for optical fiber communication systems," in *Semiconductor Devices for Optical Communication*, Springer-Verlag, New York, 1980.
9. R.L. Poulin, D.R. Pauluzzi and M.R. Walker, "A Multi-Channel Infrared Telephony Demonstration System for Public Access Applications", *Proc. of 1992 IEEE Conf. on Sel. Topics in Wireless Commun.*, Vancouver, B.C., Canada, June 25-26, 1992, pp. 286-292.
10. G. Yun and M. Kavehrad, "Spot Diffusing and Fly-Eye Receivers for Indoor Infrared Wireless Communications", *Proc. of 1992 IEEE Conf. on Sel. Topics in Wireless Commun.*, Vancouver, B.C., Canada, June 25-26, 1992, pp. 286-292.
11. R.T. Valadas and A.M. de Oliveira Duarte, "Sectored Receivers for Indoor Wireless Optical Communication Systems", *Proc. of 5th IEEE Intl. Symp. on Personal, Indoor, and Mobile Radio Communications*, The Hague, Netherlands, September 21-23, 1994.
12. J.G. Proakis, *Digital Communications*, Third Edition, McGraw-Hill, New York, 1995.
13. M. D. Kotzin, "Short-Range Communications Using Diffusely Scattered Infrared Radiation", Ph.D. Dissertation, Northwestern University: Evanston, IL, June 1981.
14. B.E.A. Saleh and M.C. Teich, *Fundamentals of Photonics*, J. Wiley & Sons, New York, 1991.